Egyptian Journal of Petroleum 31 (2022) 89–94

HOSTED BY

Contents lists available at ScienceDirect

Egyptian Journal of Petroleum

journal homepage: www.sciencedirect.com

Full Length Article

Triple aging of the RRA Al -Cu 2024 alloy and its impact on the mechanical and microstructure properties ☆

Y. Reda [a], H.M. Yehia [b], A.M. El-Shamy [c,*]

[a] Chemical Engineering Department, Canal High Institute of Engineering and Technology Suez, Egypt
[b] Production Technology Department, Faculty of Technology and Education, Helwan University, Cairo, Egypt
[c] Physical Chemistry Department, Electrochemistry and Corrosion Lab., National Research Centre, El-Bohouth St. 33, Dokki, P.O. 12622, Giza, Egypt

ARTICLE INFO

Article history:
Received 19 June 2022
Revised 18 August 2022
Accepted 28 August 2022

Keywords:
Retrogression re-aging RRA
Microstructure
Scanning electron microscope SEM
Al Cu −2024 alloy
Heat treatment
Electron diffraction X-ray EDS

ABSTRACT

The thermal–mechanical technique presented in this paper has been developed to increase the intensity and ductility of the Al-2024 alloy. As a result of standard solid solution treatment, cold rolling at room temperature, and imitation maturing at 175 °C for three hours. After aging, the Al 2024 alloy has ultimate and yield strengths at 469 MPa and 324 MPa, correspondingly. The microstructure and malleable features of an extruded Al 2024 alloying combination have been investigated in the manner of heat treatment T6. SEM, X-ray diffractometry, and optical microscopy were all used to examine the microstructure of the alloy under study. Aluminum Al 2024 alloy was established on the synthesis of rich copper intermetallic. There was a comparison of several mechanical properties since following the protrusion and heat treatment T6, researchers observed that A2024 had considerably enhanced tensile properties. Researchers found that the composite exhibits elongation of the decisive intensity and values of 381 MPa and 13.6 %, individually. An examination of the rupture exteriors of hot-squeeze-out composite specimens exposed that the malleable form of rupture predominates. Triple aging is the third aging process after the third heat treatment process, which takes place in either artificial or natural aging.

1. Introduction

During the past decade, nanostructure and ultrafine grain of aluminum alloys have been the focus of various studies concerned with exosphere and vehicle presentations [1–3]. Strength and ductility are two of the most significant mechanical qualities of structural aluminum alloys. Tensile elongation of more than 5 % is required for structural applications of the high-strength aluminum alloy at room temperature. However, they are often found inversely proportional to one another [4]. You may use various ways to create finely structured materials, which can be grouped into two categories: the consolidation of nanostructured powders of the yield materials [5–8]. This is because mechanical characteristics like module, 0.2 % resistant tension, and elongation intensity might improve. When tensile ductility and fracture toughness increase, the other properties often drop [9]. Owing to its handling elasticity, minimal compactness, excellent resistance wear, the capacity of heat healing, and increased modulus of flexibility and intensity, the matrix composites of Al-based have numerous uses, largely in the exosphere and motorized sectors [10–12]. These composites are made in various ways, most commonly are type casting and application of powder metallurgy [13–15]. Because standard casting equipment has been employed regardless of the size or shape of the component, casting methods are simple and cost-effective [16]. Extruded specimens had elongation and decisive intensity values of 18.5 % and 145 MPa, compared to uncast specimens with just 3.5 % and 54 MPa [17]. Material strength and microstructure, which may be determined by a suitable manufacturing method, determine metal matrix composites (MMCs), and ultimate tensile characteristics. The precipitation of the conversion segment and subsequent developments in mechanistic characteristics after solution treatment and aging operations have attracted attention to these alloy systems. Al-Cu alloys have been employed to modify the alloying matrix and improve the technical features. The Al 2024 after gibbousness and heat treatment T6 have been compared for microstructure and tensile properties in this study [18]. This research aims to develop a better approach for simultaneously improving intensity and ductileness and evaluating the mode of action involved in the process. With the combination of solid solution treatment and cold rolling at ambient heat, concerning the unnatural aging methods, it was feasible to develop

Peer review under responsibility of Egyptian Petroleum Research Institute.
* Corresponding author.
E-mail address: am.elshamy@nrc.sci.eg (A.M. El-Shamy).

https://doi.org/10.1016/j.ejpe.2022.08.003
1110-0621/

the alloy of Al-2024. Dissimilar handling circumstances have been used to evaluate the malleable possessions of the alloy of Al-2024 [19].

2. Materials and methods

The alloy under study is the powder of commercial alloy of Al-2024 comprising extra elements with proper % used as a starting material as seen in Table 1. The Sumitomo model NO. 1020SPS has been employed to consolidate the samples. Graphite dies being sliced with two punches have been in an experiment. The punches were designed to be 15 mm in diameter and 25 mm in length. It took 100 min of heating to achieve 500 °C, and 50 MPa pressure has been applied.

The sintering duration was ten minutes, according to the manufacturer's instructions. In the following, sample 1 has used to refer to such a sample. Solid solution treatment (SST) and a vacuum furnace have been carried out for 1 h on sample 1. The substances were promptly treated in water at 25 °C to complete the assessment procedure and will be named sample 2 from now on. At room temperature after SST, a cold rolling process was done to lower the stiffness from 4 mm to 2 mm, with a 0.1 mm decrease for each pass. The anisotropy in mechanical characteristics is averted by alternately rolling in diagonal and longitudinal directions. We will name it sample 3 from now on. Temperatures of 175 °C for 3 h and 100 °C for 18 h were used to maximize the strength and ductility of the cold-rolled samples. They will be referred to sample 4 and sample 5 from now on. Notably, standard heat treatment methods have chosen the maturing heat and duration in this paper on Al alloys from the 2xxx series, together with more recent research. The mechanical features of the samples were established utilizing Vickers micro-hardness and tensile assessments. To minimize surface residual stress, all tests were cleaned using aggressive emery paper and suspension of silica before carrying out the test. A SHIMADZUHMV-1 T micro-hardness tester has been used with 100 g load and 15 *sec* to test Vickers micro-hardness. All these numbers are centered on the average of 15 indentation marks. The selected materials were cut off and refined into dog-bone samples with measure lengths of 3 mm and cross-sections of 1x1 mm to evaluate their strength. As the testing machine was computer-controlled, it was possible to capture load and digital displacement data. Tested at unique conditions of a virtual-stationary level of the strain of $5X10^{-4}$ s^{-1}, displacement of the ductile gauge segment was directly measured using a dual-photographic camera with extensometer video to assess a material's strength and ductility, we typically utilize three samples. Researchers examined thin foil tests employing (SEM&EDS) on a JEM 2100 electron microscope running at 200 kV (EDS) [20].

Table 1
Chemical analysis of Al-2024.

Cu	Mn	Mg	Si	Cr	Ti	Zn	Al
4.4	0. 6	1.5	0.5	0.1	0.05	0.2	Rem

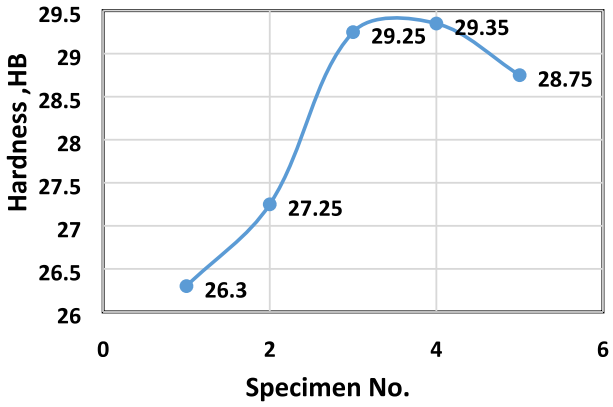

Fig. 1. The values of the alloy's microhardness and its mechanical characteristics at T6T7 and RRA correspond to the parameters listed in Table 2.

3. Results and discussion

3.1. Mechanical properties

In Fig. 1 and Table 2, you can see the typical curves of stress–strain and values of the mechanical characteristics for the Al-2024 alloy at several production stages. The heat-treated T3, T4, and T8 of the alloy of Al-2024 for their greatest malleable intensity generate intensity and elongation. Its strength was 280.5 MPa, its ultimate 452.8 MPa, and its extension to collapse was 27.3 % after one hour at 493 ^{0}C, suggesting that SST significantly increased the intensity of the alloy Al-2024. Additionally, the above outcome is more than it is also significantly superior to the SST modeling composite in terms of performance and durability. SPS alloy has been chosen instead of traditional cast metal for this purpose. When examining the optical images, sample 1 has a median particle mass of approximately 5 μm, much smaller than that found in most cast alloys. Its strength and ultimate have been raised to 501.2 and 553.4 MPa, respectively, by cold rolling sample 2. Because of this, the necking process proceeds fast once a maximum stress value is reached, and the sample 3 specimen elongates uniformly at just 4.9 % and fails at 8.9 %. After yielding in the cold-worked material, a minor strain hardening is responsible for reducing tensile ductility [21–23]. This component layer has a claimed malleable extension-to-collapse of less than 4.5 %. However, after 18 h at 100 °C, sample 3′s is around 40 MPa smaller than test 3. Intriguingly, test 3′s strength and ductility have simultaneously been enhanced by 3 h of aging at 175 °C. Until now, this hasn't been proven. The strength

Table 2
Heat remedy for Al-2024.

Sample no.	Solution Remedy		Artificial Aging	Artificial Aging		Precipitation		Artificial Aging	
	T, °c	t, (hr)		T, °c	t, h	T, °c	t, h	T, °c	t, h
1	495	20 m	Water	180	6 h	190	12 h	180	6 h
2	495	20 m	Water	180	6 h	190	12 h	RT	5 d
3	495	20 m	Water	RT	5 d	190	12 h	180	6 h
4	495	20 m	Water	RT	5 d	190	12 h	180	6 h
5	495	20 m	Water	RT	5 d	190	12 h	RT	5 d

RT = Room Temperature, T = Temperature, t = Time, d = day h = hour m = min.

value is 529.6 MPa, the ultimate value is 583.1 MPa, and the elongation to failure is 16.2 %. According to the manufacturer, the strength is 28.4 MPa stronger than sample 3 and over 200 MPa stronger than the usual heat-treated T3 and T4 of the alloy Al-2024. There are several different types of Al-2024. Table 2 further summarizes the Vickers micro-hardness variation under different processing circumstances. The alloy's Vickers micro-hardness and strength values were highest after three hours of aging at 175 °C. Because our results match Vickers micro-hardness and yield strength YS, we may be certain that our findings are reliable. Deformations localized in a similar plane were also governed, in part, by the considered criteria [24].

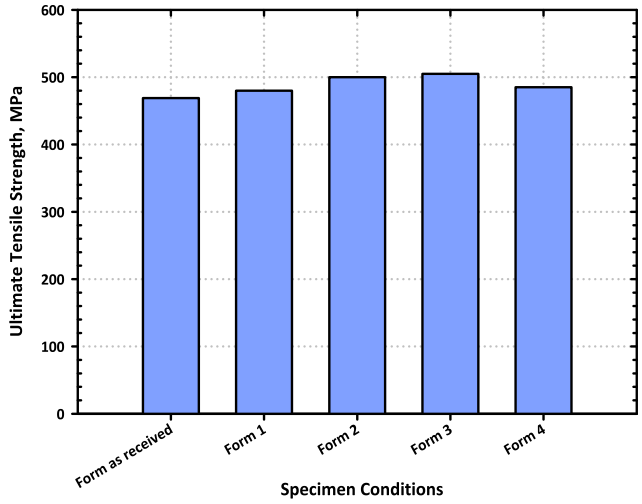

Fig. 2. Tensile qualities of Al-2024 sheets after they have been aged in a variety of various approaches, involving untreated and treated for the malleable properties of the whole development after it has been aged under a variety of different situations.

$$\left(\frac{\partial\sigma}{\partial\varepsilon}\right)_{\cdot\varepsilon} = \sigma \tag{1}$$

Where the genuine stress is σ and the true strain, ε.

Substantial work hardening has occurred in samples 4 and 5 compared to other cold-worked or UFG materials and alloys tested. Examples include sample 4′s 9.5 % uniform lengthening, almost twice as much as the sample without age. Because of a higher work-hardening rate, which can be premeditated using Eq (2):

$$\theta = \frac{1}{\sigma}\left(\frac{\partial\sigma}{\partial\varepsilon}\right)_{\cdot\varepsilon} \tag{2}$$

The normalized work hardening rate curves are shown in Fig. 1 versus the real strains in the experiment. There is a significant difference between the sample's ductility after aging and the unaged samples.

An improvement in yield strength by 29 MPa has been achieved by using a superior bulk of nano-sized S′-level hastens. As mentioned in Fig. 2, we can see that sample 3′s uniform elongation has increased with age. Since grain expansion during maturation can undoubtedly enhance ductility, we assume its influence should be resulting in this situation. After maturation, the particle sizing is even now extremely fine approximately 213 nm. Ductility of the skin increased significantly with age because of these three microstructural changes. For the second reason, following aging, there is significant room for displacement buildup before dissemination through the malleable assessment since it can prolong the development of smooching and enhance the effort-hardened level [25]. This alloy's work-hardening rate has been improved due to

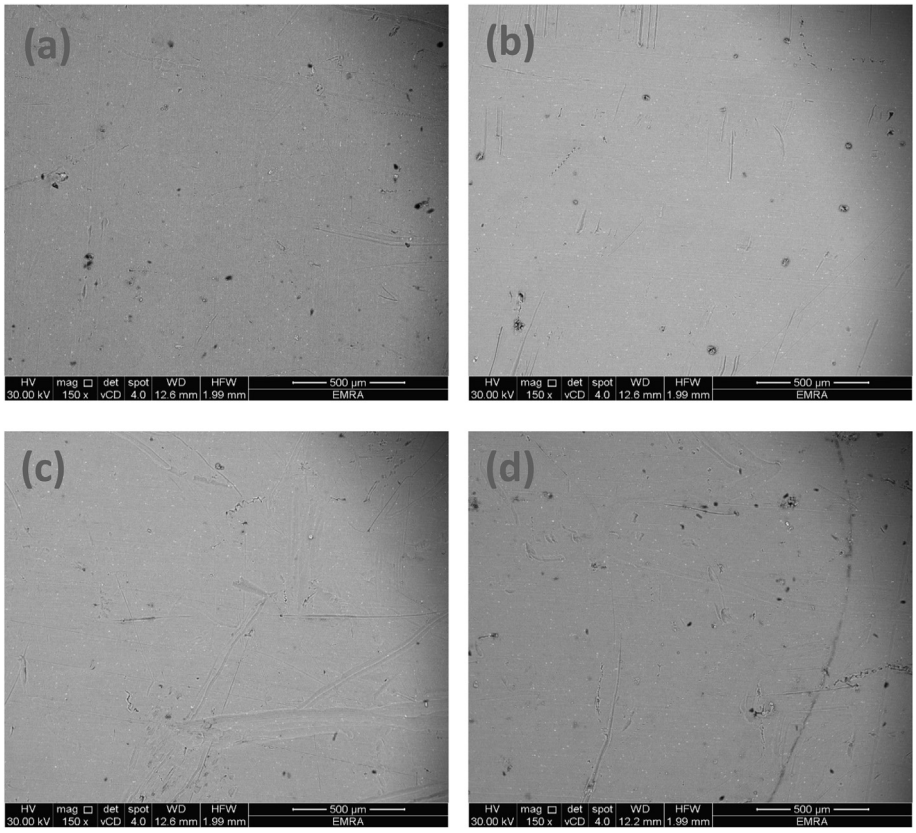

Fig. 3. SEM micrograph for heat-treated Al-Cu alloy 2024 by (a) Form 1 (b) Form 2 (c) Form 3 (d) Form 4 produced from Table 2.

the high density of nano-sized S′ precipitates. According to the literature, the dislocation density of Al 7075 alloy after tensile testing increased by 54 % above its undeformed condition [26,27]. Dislocation density increased by just 8 % when compared to an alloy that did not include any phases. During aging, we observed three microstructural changes that enhanced the ductility of the Al-2024 alloy.

3.2. Microstructure

We could look into mechanical properties with microstructure by examining the microstructure and precipitate formation on samples under different processing conditions. On the bright field SEM image in Fig. 3a-d, we can see the microstructure of sample 2. A modest number of dislocations are present in the system. It is possible to identify leftover particles in Al grain using EDS and SAED (Al 20 Cu 2 Mn 3). When limiting grain development during heat treatments, the dispersed *T*-phase performed a vital and favorable function. The *T*-stage fragments are also efficient in displacement trapping and buildup through CR, according to prior studies. Fig. 3a illustrates the sample's microstructure and the high dislocation densities that were entrapped across the *T*-stage fragments following a high rolling strain. The changeable mass is significantly smaller in the absence of *T*-fragments. Fig. 3b-d represent the SEM of treated samples under different conditions as mentioned in Table 2 and it is noticed that the surface became much better compared with the untreated surface. There is evidence that the *T*-phase is still active during CR because of the varying dislocation density.

The little sparks deflection locations of the Al [001] region in the highest left inset imply that sub-grain structures with minor misorientation have been generated during cold working at ambient temperature [28–30]. It is established by the EDS assessment as demonstrated in Fig. 4a, b, which shows that the grain size has been decreased by cold rolling. There are several ways to simplify the Hall-Williamson equation [31–33].

$$B\cos\theta = \frac{K\lambda}{D} + 2\varepsilon\sin\theta \tag{3}$$

B is the peak width of the at half extreme; K is the constant of Scherrer (supposition K140.9); D is the secondary-particle mass; the strain of the lattice; λ is the wavelength of X-ray radiation; and θ is the angle of Bragg.

For sample three, it has been discovered that the secondary-particle mass and the pattern species were 114 nm and 0.58 %, correspondingly. Following 3 h at 175 °C, the secondary-particle mass was thickened to 213 nm, and the pattern species diminished to 0.25 %. FCC's unique rolling texture causes a significant reduction in peak strength except for the (220) peak and the lack of other peaks (e.g. (311). By combining the median particle sizing D and

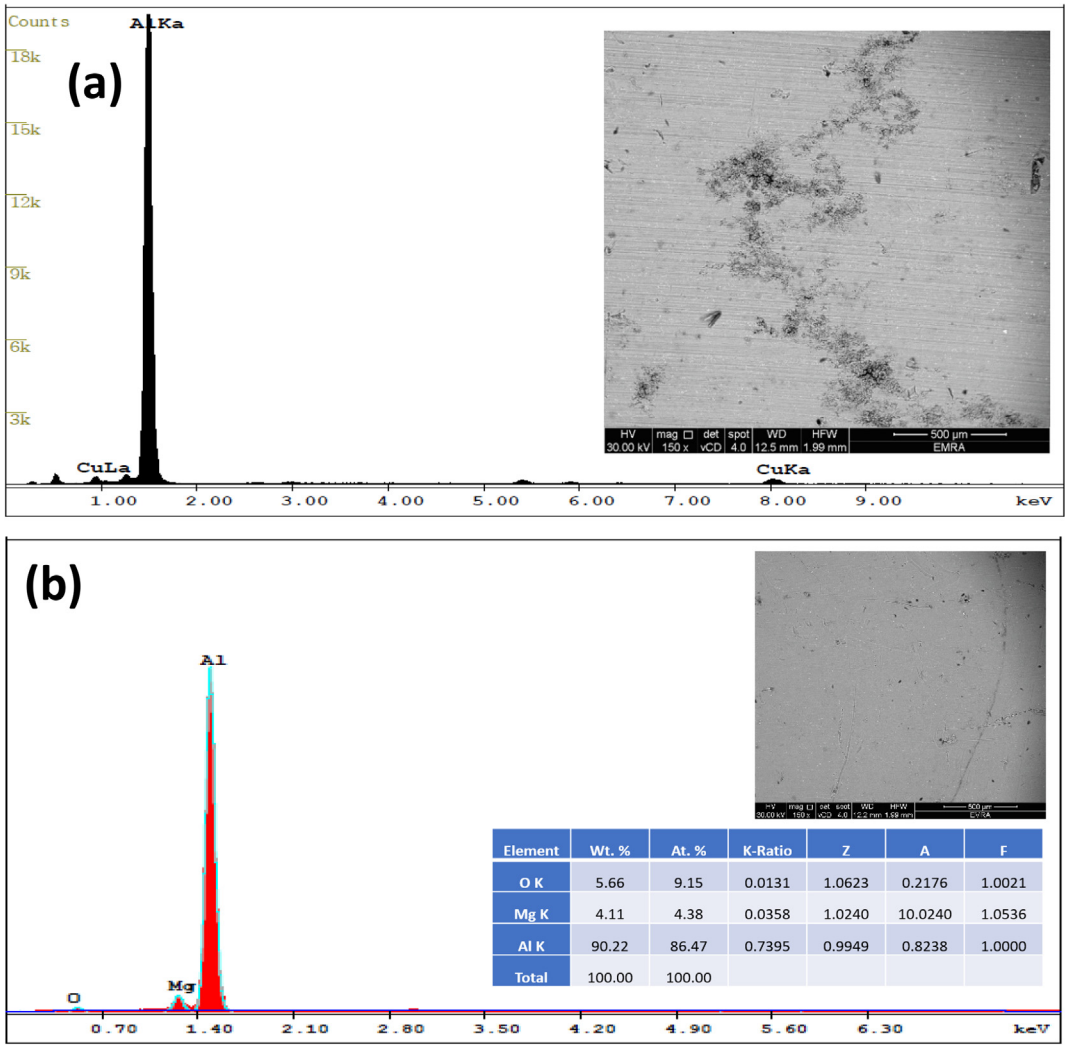

Element	Wt. %	At. %	K-Ratio	Z	A	F
O K	5.66	9.15	0.0131	1.0623	0.2176	1.0021
Mg K	4.11	4.38	0.0358	1.0240	10.0240	1.0536
Al K	90.22	86.47	0.7395	0.9949	0.8238	1.0000
Total	100.00	100.00				

Fig. 4. SEM-EDS for Al-Cu alloy 2024 by heat treatment (a) before heat treatment (b) after treatment under condition (4).

the pattern species, you can also calculate the dislocation density [34–36].

$$\rho = \frac{2\sqrt{3\varepsilon}}{Db} \tag{4}$$

b gives the Burger's vector (0.286 nm for aluminum). Fig. 4b shows the findings of SEM and EDS for sample 4.

A significant concentration of nano-shaped pine needle-designed hastens has been detected (Fig. 4b), but the number of clearly outlined dislocation cells was greatly diminished, suggesting a remarkable drop in displacement intensity. Fig. 4b shows spacing dissemination in the fragmented segment and entomb-grain for the residues centered on the micrograph of the SEM pictures. Fragment distance and interparticle separation are estimated to be 31.6 and 28.9 nm, respectively. On the High-resolution transmission electron microscopy HRTEM image (Fig. 4b) at [001] Al, the second phase particles were detected, as well as the matching SEAD pattern (Fig. 4b). The pattern of A 001-horizontal obsession along with the aluminum indicates that the spine-molded occasions are the S′ (Al-2-Cu-Mg) phases. When it comes to Al-Cu-Mg alloys, S′ phase is a major strength-enhancer. It is found that the A cool-produced and matured Al-2024 alloy also has a similar microstructure and SEAD pattern [35–37].

3.3. Mechanics of microstructure

It is well-known that the cold rolling technique produces secondary textures and a superior intensity of displacements. This means that dislocation density and grain refinement have a significant character in deciding the strength of cold-rolled steel in its final form. Additionally, in the aging process, three microstructural changes occurred. Cold rolling should have weakened the model and relieved core tension. As a result, their sample's strength is believed to be compromised. Another study proved this by proving that the second-phase particle scan can withstand the slipping of dislocations during tension testing. A third component is a large concentration of nano-scaled S-stage hastens. To compensate for this test, the sample 5 yield strength has been reduced by 40 MPa direct to texture development and displacement intensity reductions [38–40].

3.4. Strengthening mechanisms

In this section, we'll examine and explain the mechanisms that contribute to the high potency of the samples. The fourth heat treatment condition exhibits precipitous growth of intensity, displacement increase, as well as texture improvement support based on all their microstructural characteristics and parameters acquired by SEM and EDS. It assessed the total strength by applying intensity growth assumptions to ascertain the quantifiable provisions of their various mechanisms of strengthening. As a result, their material's intensity is increased. Using this method, you may boost your power.

$$\Delta\sigma Or = \varphi\frac{Gb}{L} \tag{5}$$

The shear modulus G, the Orowan mechanism strength increase sOr, and Burger's vector b. There are millimeters between each precipitation measured by L. Orowan strengthening, for example, would add 259.3 MPa to the entomb-fragment spacing of about 28.9 nm, as well as the shear modulus is about 26.2-GPa, and Burger's direction of 0.286 nm. Direct to their development of displacements throughout the process of cool rolling, dislocations get stronger. As an alternative, the Taylor formula may be used to analyze the data [41–43]:

$$\Delta\sigma_{dis} = \delta GB\rho^{\frac{1}{2}} \tag{6}$$

Sdis = Strength Increase Due to Dislocation Strengthening; G and b have the same importance as before, and the constant of 0.22 (C) grain refinement strengthening. The dislocation density is calculated by Eq. of the Hall-Petch relationship [44–46].

$$\Delta\sigma H - p = \varphi\frac{K_y}{\sqrt{D}} \tag{7}$$

In the case of Al alloys, Ky is a constant of order 0.1 MPa. In this case, D stands for grain size D set to 213 nm would result in 216.7 MPa of grain refinement contribution. So, the whole intensity of this test is computed. The following formula may calculate the yield strength of sample 4 (sample 4):

$$\Delta\sigma sample4 = \sigma_0 + \Delta\sigma_{Or} + \Delta\sigma_{dis} + \Delta\sigma H - P \tag{8}$$

The alloy Al-2024 in its annealed condition (s0) with 75 MPa yields strength. This is in satisfactory accord including the investigational finding of about 529.6 MPa. If you overemphasize texture delicacy improving because the XRD patterns determine a consistent deflection sphere dimension, since it is secondary texture/displacement of the group dimension, then you will overestimate the yield strength [47–60].

4. Conclusions

This work exhibits a technique of thermo-mechanical which instantaneously improves the intensity and ductileness of Al-2024 alloy conclusively. The engineering of this technique produces intensity and supreme malleable powers of about 529.6 and 583.1 MPa, correspondingly. Dislocation density, grain refinement, and an equally distributed high density of nanosized S precipitates are responsible for the alloy's excellent mechanical properties. A better quantitative knowledge of the link between yield strength and microstructure may also have been used to design high-performance precipitation-strengthened alloys. The optimal heat treatment settings for the gradient composite are summarized in solution treatment at 49 °C for 45 min, water quench, and artificial aging at 185 °C for 12 h. During the transition zone of the alloy Al 2024, both long- and short-range diffusion occurs. There are two primary processes in solution treatment: dissolving of the intermetallic compound and homogenization of micro-segregation. Short-distance diffusion, coupled with precipitation response, is the most important at this stage. Because it is strongly reliant on the temperature and time of the solution, long-distance diffusion is poor.

Declaration of Competing Interest

The authors declare that they have no known competing financial interests or personal relationships that could have appeared to influence the work reported in this paper.

References

[1] Y. Reda, H.M. Yehia, A. El-Shamy, Egypt. J. Pet. 31 (2022) 9–13.
[2] T.H. Fang, W.L. Li, N.R. Tao, K. Lu, Science 331 (2011) 1587.
[3] L. Lu, X. Chen, X. Huang, K. Lu, Science 323 (2009) 607.
[4] B. Ateya, F. Alkharafi, A. El-Shamy, A. Saad, J. Appl. Electrochem. 39 (2009) 383–389.
[5] K. Zohdy, R. El-Sherif, A. El-Shamy, Upst. Oil Gas Tech. 2021 (6) (2021) 100025.
[6] R.Z. Valiev, R.K. Islamgaliev, I.V. Alexandrov, Prog. Mater. Sci. 45 (2000) 103–189.
[7] D.B. Witkin, E.J. Lavernia, Prog. Mater. Sci. 51 (2006) 1–60.
[8] H. Farag, A. El-Shamy, S. El Abedin, Z. Phys, Chem. 230 (12) (2016) 1733–1744.
[9] Ashraf K. Eessaa1, A. M. El-Shamy Y. Reda, Egypt. J. Chem. 2018; 61(1): 175-185.
[10] R.Z. Valiev, Nature 419 (2002) 887–889.

[11] C. Suryanarayana, Prog. Mater. Sci. 46 (2001) 1–184.
[12] Y. Reda, K. Zohdy, A. Eessaa, A. El-Shamy, Egypt. J. Chem. 63 (2) (2020) 579–597.
[13] D.L. Zhang, Prog. Mater. Sci. 49 (2004) 537–560.
[14] I. Abdelfattah, W. Abdelwahab, A. El-Shamy, Egypt. J. Chem. 65 (2) (2022) 687–694.
[15] M. Shehata, N. Ammar, A. El-Shamy, Egypt. J. Chem. 62 (9) (2019) 1587–1602.
[16] A. Abd Elkarim, A. El-Shamy, M. Megahed, A. Kalmouch, Arctic J. 71 (1) (2018) 2–33.
[17] R.Z. Valiev, Nat. Mater. 3 (2004) 511–516.
[18] K.M. Shorowordi, T. Laoui, L. Froyen, J. Mater. Process. Technol. 142 (2003) 738–743.
[19] Y. Reda, A.M. El-Shamy, A.K. Eessaa, Ain Shams Eng. J. 9 (2018) 2973–2982.
[20] L. Balogh, R. Figueiredo, T. Ungar, T. Langdon, Mater. Sci. Eng. A 528 (2010) 533.
[21] S. Zhiqiang, Z. Di, L. Guobin, Mater. Design. 26 (2005) 454–458.
[22] E. El-Kashef, A. El-Shamy, A. Abdo, A. Gado, Egypt. J. Chem. 62 (8) (2019) 1467–1481.
[23] H. Arik, Y. Ozcatalbas, M. Turker, Mater. Design. 27 (2006) 799–804.
[24] M. Azarbarmas, M. Emamy, M. Alipour, J. Mater. Sci. 46 (2011) 6856–6862.
[25] D. Zhao, X. Liu, Y. Liu, X. Bian, J. Mater. Sci. 40 (2005) 4365–4368.
[26] A. El-Shamy, M. Shehata, H. Metwally, A. Melegy, Silicon 10 (6) (2017) 2809–2815.
[27] A. El-Shamy, I. Abdelfattah, M. Shehata, J. Environ. Manag. 219 (2018) 325–331.
[28] T.S. Srivatsan, J. Mater. Sci. 31 (1996) 1375–1388.
[29] Y. Kang, S. Chan, Mater. Chem. Phys. 85 (2004) 438–443.
[30] R. Rahmani Fard, F. Akhlaghi, J. Mater. Process. Technol. 2007; (187-188): 433-436.
[31] M. Megahed, M. Youssif, A. El-Shamy, Egypt. J. Chem. 63 (12) (2020) 5269–5287.
[32] A.M. El-Shamy, H.K. Farag, W.M. Saad, Egypt. J. Chem. 60 (6) (2017) 1165–1175.
[33] K. Tavighi, M. Emamy, A.R. Emami, Mater. Design. 46 (2013) 598–604.
[34] K. Tavighi, M. Emamy, Z. Tanhaee, S. Vaziri, Mater. Sci. Eng. A. 606 (2014) 92–100.
[35] A.M. El-Shamy, M.M. Abdel Bar, Egypt. J. Chem. 64 (4) (2021) 1867–1876.
[36] A. M. El-Shamy, (2020). Egypt. J. Chem. 2020; 63(12): 5251-5267.
[37] A. Albiter, C. Leon, R.L. Drew, E. Bedolla, Mater. Sci. Eng. A. 289 (2000) 109–115.
[38] E.W. Hart, Acta Metall. 15 (1967) 351–355.
[39] D. Jia, Y. Wang, K. Ramesh, E. Ma, Y. Zhu, R. Valiev, Appl. Phys. Lett. 79 (2001) 611.
[40] M. Megahed, M. Abdel Bar, A. El-Shamy, Egypt. J. Chem. 64 (10) (2021) 5693–5702.
[41] K. Zohdy, R. El-Sherif, A. El-Shamy, J. of Bio-Tribo-Corrosion 7 (2) (2021) 1–7.
[42] Y.H. Zhao, X.Z. Liao, Z. Jin, R.Z. Valiev, Y.T. Zhu, Acta Mater. 52 (2004) 4589.
[43] Y.H. Zhao, X.Z. Liao, S. Cheng, E. Ma, Y.T. Zhu, Adv. Mater. 18 (2006) 2280.
[44] X.H. Chen, L. Lu, K. Lu, Scr. Mater. 64 (2011) 311.
[45] A. El-Shamy, M. El-Hadek, R. El-Bindary, Mor. J. Chem. 8 (4) (2020) 788–800.
[46] Amal M. Abdel Karim, A. M. El Shamy, J. of Bio- and Tribo-Corrosion 2022; 8:35.
[47] H. Wen, T. Topping, D. Isheim, D. Seidman, E. Lavernia, Acta Mater. 61 (2013) 2769.
[48] M. Abbas, K. Zakaria, A. El-Shamy, Z. Phys, Chem. 235 (4) (2019) 377–406.
[49] R. El-shiekh et al., J. Ethnopharmacol. 238 (2019) 111893.
[50] Y. Zhu, J. Huang, J. Gubicza, T. Ungar, R. Valiev, J. Mater. Res. 18 (2003) 1908–1917.
[51] M. Abbas, A. Ismail, K. Zakaria, S. El Abedin, Sci. Rep. 12 (2022) 12536.
[52] D.A. Elsayed et al., Bioorg. Chem. 124 (2022) 105805.
[53] H. Wafaa, S. Amany, F. Hany, M. Samar, Egypt. J. Chem. 65 (9) (2022) 317–328.
[54] A.H. Atta, S.M. Mouneir, Environ. Sci. Poll. Res. 29 (11) (2022) 15282–15302.
[55] G. Yasin, M. Arif, Y. Tang, M. Nadeem, Adva. Eng. Mat. 20 (7) (2018) 1701166.
[56] G. Yasin et al., J. Alloy. Compd. 755 (2018) 79–88.
[57] G. Yasin et al., Diam. Relat. Mater. 104 (2020) 107763.
[58] G. Yasin et al., Vacuum 159 (2019) 482–493.
[59] G. Yasin et al., Arch. Civil Mechan. Eng. 19 (4) (2019) 1484–1496.
[60] G. Yasin et al., Mater. Charact. 157 (2019) 109901.